Spike protein fusion loop controls SARS-CoV-2 fusogenicity and infectivity

Debnath Pal*

Department of Computational and Data Sciences, Indian Institute of Science, Bengaluru, Karnataka-560012, India

*Corresponding Author: dpal@iisc.ac.in

Running Title: Fusion peptides in SARS-CoV-2 spread

Abstract

The Spike is a hallmark coronavirus protein that determines virus fusion, entry and spread in the host, and thus holds clues for the rapid spread of the SARS-CoV-2 pandemic. We have investigated the Spike from six β-coronaviruses, including the SARS-CoV-2, and find that their surface-exposed fusion peptides constituting the fusion loop are spatially organized contiguous to each other to work synergistically for triggering the virus-host membrane fusion process. The SARS-CoV-2 fusion peptides have unique physicochemical properties, accrued in part from the presence of consecutive prolines that impart backbone rigidity which aids the virus fusogenicity. The specific contribution of these prolines has been inferred from comparative studies of their deletion mutant in a fellow murine β-coronavirus MHV-A59 that show significantly diminished fusogenicity *in vitro* and associated pathogenesis *in vivo*. The Spike cleavage-linked priming and fusogenic conformational transition steered by the fusion loop may be critical for the SARS-CoV-2 spread.

Keywords: coronavirus; SARS-CoV-2; fusion peptide; COVID-19; Spike glycoprotein; MHV-A59; two consecutive prolines; structural rigidity

Summary. The Spike protein on the SARS-CoV-2 surface is the prime mediator of COVID-19[1] because of its central role in virus-host attachment, virus-entry, and virus-spread[2]. The contagious nature of SARS-CoV-2 infection has been attributed to dense glycosylation of the Spike glycoprotein[3], its high affinity of binding to human ACE2 receptor[4], and cleavage[5]. While these may be imperative, it does not explain the uncontrolled infectivity. Here we show that properties of the fusion peptides constituting the fusion loop of SARS-CoV-2 Spike that triggers the virus fusion, distinguishes it from the other five β-coronaviruses. The SARS-CoV-2 Spike trimer surface is relatively more hydrophobic, including the surface contributed by the fusion peptides. The fusion peptides are structurally rigid owing to its consecutive prolines, aromatic/hydrophobic clusters, a stretch of consecutive β-branched amino acids, and the hydrogen bonds. The role of rigidity accrued from the presence of consecutive prolines contributing to virus fusogenicity can be deciphered from our previous murine β-coronavirus, MHV-A59 studies[6]. The synergy brought about by the global location of the surface exposed fusion peptides, their physicochemical features, and the fusogenic conformational transition appears to drive the fusion process, which may explain the severity of the infection and widespread nature of the COVID-19 pandemic.

Introduction. The novel Coronavirus Disease 2019 (COVID-19) caused by SARS-CoV-2, Severe Acute Respiratory Syndrome (SARS) by SARS-CoV, and Middle Eastern Respiratory Syndrome (MERS) by MERS-CoV, induce severe acute respiratory distress in patients. Though these diseases share similar clinical and pathological features, COVID-19 differs in overlapping yet distinct phases of infection[1,7]. The degree of infectivity is significantly high in SARS-CoV-2, and far more virulent, as evidenced by the current global pandemic. The difference may accrue early

on when a rapid viral replication ensues cell-to-cell spread, and acute inflammation begins to mount. Uncontrolled viral replication and dysregulated host immune responses may be the leading cause of fatality by SARS-CoV-2. Despite many studies, the underpinnings of high virus infectivity remain poorly understood. Therefore, it is essential to dissect the genomic control of SARS-CoV-2 infectivity and virulence for the rational designing of therapeutic agents.

The genome. The genomic constitution of SARS-CoV-2 does not appear to be unique in the background of the disease pathology. The MERS-CoV share ~51% genome sequence identity to SARS-CoV and SARS-CoV-2. Two other β human coronaviruses (HCoVs), HCoV-HKU1, and HCoV-OC43 also share ~51% genome identity to SARS-CoV and SARS-CoV-2. Yet they cause a common cold instead of acute respiratory distress. Human α-coronavirus NL63 and 229E strains which are even further diverged from the β-HCoV genomes also cause a common cold. Even essential genes like the RNA dependent RNA polymerase (RdRp) have diverged, for example, RdRp from SARS-Cov-2/SARS-Cov is only 71-72% identical to MERS-CoV (Table S1). Therefore, what gene or genomic feature(s) distinguishes each virus is an important consideration in understanding its infectivity and spread across hosts.

The Spike. Among all coronaviruses, Spike is a key gene that determines infectivity due to its established role in initiating virus-host attachment, fusion, entry, and cell-to-cell fusion post replication[3]. The expressed protein executes its function through a trimeric quaternary structure, with each monomer segmented into the S1 and S2 domains, where S1 consists of the N-terminal domain (NTD) and the C-terminal domain (CTD), while the S2 (also known as the fusion domain) consists of the fusion peptides (FPs), central helix (CH), heptad repeat regions HR1 and HR2, and a transmembrane domain (TM) followed by the cytoplasmic tail (CP) (Fig. 1A). The NTD or CTD embeds the receptor-binding domain (RBD) depending on the individual virus. In SARS-CoV-2 the CTD embeds the RBD. The RBD recognizes the host-cell and mediates the virus-host attachment, while the S2 domain drives the viral entry into the host cell and cell-to-cell fusion by catalyzing the virus-host membrane fusion process. The TM anchors the protein in the viral membrane, while the FPs contribute to the trigger that drives the virus-host membrane fusion process. A transition pathway has been proposed to proceed through a pre-hairpin intermediate structure followed by pre-bundle hemifusion membrane-associated structure, bundle structure, and the eventual post-fusion structure[8]. It is remarkable that despite their similarity in function, β-coronavirus Spike proteins have widely diverged, with the RBD diverging further (21%-61% pairwise sequence identity), explained in part by the diversity of its host receptor targets like the human ACE2 for SARS-CoV and SARS-CoV-2, DPP4 for MERS-CoV, and 9-O-Ac-Sia for HCoV-OC43 and HCoV-HKU1. The S2 domain has also diverged, but comparatively less with >33% overall pairwise sequence identity – the heptad repeat regions being the most conserved (Fig. 1B). It is pertinent to ask what features of Spike sequence and structure determine the virus fusogenicity and infectivity.

Spike glycosylation. Densely glycosylated Spike protein has been suggested as the prime reason for the high SARS-CoV-2 infectivity[3]. This extensive glycosylation of the S2 domain is driven by an intracellular N-terminal signaling peptide for transport and retention in the endoplasmic reticulum (see Fig. 1B Multiple Sequence Alignment[9] bottom panel). However, this signal

sequence is absent in a fellow murine β-coronavirus MHV-A59 Spike protein[10], indicating limited glycosylation. Yet, MHV-A59 aggressively infects the mouse liver and brain. Upon intracranial inoculation in mice, it can cause acute stage meningoencephalitis and myelitis, chronic stage demyelination, and axonal loss[11-13]. It infects the neurons profusely and can spread from neuron to neuron. Its propagation from grey matter neuron to white matter and release at the nerve ends to infect the oligodendrocytes by cell-to-cell fusion[12] are robust mechanisms to evade immune responses and induce chronic stage progressive neuroinflammatory demyelination concurrent with axonal loss in the absence of functional virions[12,14]. Therefore, high infectivity of the MHV-A59 Spike does not appear to be contingent on glycosylation and one can argue the same for SARS-CoV-2 Spike, where its glycosylation may only marginally raise the basal fusion efficiency. Surface glycosylation thus may not be a contributing factor to host cell binding, although the successive virus-to-cell and cell-to-cell fusion may all-together play an important role in higher virus infectivity.

Spike receptor binding. It has been suggested that enhanced virus-to-cell infection can be propelled by the increased number of hydrogen-bonded contacts between SARS-CoV-2 RBD and ACE2 receptor leading to higher affinity and improved host targeting compared to the SARS-CoV[3,4]. However, such a proposition is weak because the RBDs in all HCoVs are diverse, including SARS-CoV, where the minimal RBD (318 to 510 residues) shares only 74% sequence identity with SARS-CoV-2 (Fig. S1). Besides, a significantly higher affinity between ACE2 and SARS-CoV-2 has not been experimentally corroborated[15]. Also, the SARS-CoV-2 Spike may interact with other receptors such as DC-SIGN and DC-SIGNR as in SARS-CoV to increase tropism[16] and viral spread. Therefore, there is no direct consequence of ACE2 recognition with infectivity unless a virus entry can be realized; however, when RBDs interact with ACE2 in large numbers during the acute stage of the infection, they may modulate the host immune response by downregulating hydrolysis of the pro-inflammatory angiotensin II to anti-inflammatory angiotensin 1-7 in the renin-angiotensin signaling pathway[17]. This can alter the immune response and increase infectivity. But such effects can manifest only beyond the early stage of the infection, and for that to happen the efficiency of viral entry is the rate-limiting step.

Spike cleavage. The cleavage of the Spike protein is said to prime it for the virus-host membrane fusion process. How essential is this for virus fusogenicity and infectivity is an important consideration. The Spike cleavage potentially removes any *in situ* covalent and noncovalent constraints that the S1 domain may impose on the S2 domain impeding its conformational transition that facilitates the virus entry. The comparison of the S1/S2 cleavage signal sequence shows that SARS-CoV-2 has an "RRARS" Furin recognition site, similar to MHV-A59 Spike's "RRAHR" required for activity[5] (Fig. 1B). In contrast, the canonical cleavage recognition sequence is missing in SARS-CoV with only a single arginine present there. A regular cleavage at this site has not been reported, and cleavage by trypsin has been shown to activate the virus independent of the pH. The cleavage site signal at S2' is highly conserved across all HCoVs in contrast to the S1/S2 cleavage signal (Fig. 1B). The importance of this region has been aptly corroborated by S2' site cleavage studies in SARS-CoV[18]. Besides, it is also possible for Spike to be activated by the low pH environment through protonation of residues if it internalizes in the endosome post interaction with the host receptor. On the contrary, fusion processes are known to

happen in MHV-A59 Spike without cleavage as well[19]. Therefore, the SARS-CoV-2 Spike appears competent to access multiple pathways for priming that enhances its infection capability, including the possibility that it can infect without a cleavage as well.

Spike fusion peptides. Among all the components of the fusion apparatus in the Spike S2 domain, the FPs are the least studied although they have been suggested to contribute to the trigger that drives the virus-host fusion process by initiating the protein-host membrane contacts. Limited experimental information available shows mutation in FP of SARS-CoV Spike can significantly perturb the fusion efficiency[20] as much as >70%[21]. Most studies of the FP regions have used synthetic peptides in a fusion assay system to understand their membrane perturbing capabilities[22-25], and how Ca^{+2} ions may interact with these peptides to modulate fusion[8]. Interestingly, the FPs also contains a central proline[26] in several viruses such as the Avian Sarcoma/Leucosis virus[27], Ebola virus[28], Vesicular Stomatitis virus[29], and Hepatitis C virus[30], where its important role has been investigated through mutation studies. The location of coronavirus FPs proximal to the N-terminal of the S2 domain is reminiscent of FPs from HIV-1, influenza virus, and paramyxoviruses. They have been suggested to be at the head a pre-hairpin intermediate structure[31] predicted for the current model of class I viral fusion proteins.

Spike fusion loop. Given that FPs are believed to the early initiators of protein and host membrane contact there is still no consensus on their location. For example, the fusion peptide for SARS-CoV-2 Spike has been cited at 788-806 position by Xia et al.[32] compared to 816-833 by Wrap et al.[3]. When inferred from alignment to SARS-CoV Spike, two additional FP segments at 875-902 position and 1203-1220 can be proposed based on experimental studies by Ou et al.[33] and Guillén et al.[23], respectively. In reality, all four Spike fusion domain segments (FP-I to FP-IV; Fig. 1B) mentioned can be identified by a simple window-based analysis using interfacial hydrophobicity scales such as from Wimley and White[34]. Given that FP-1 to FP-III are contiguous to each other in the sequence, the whole segment spanning the beginning of FP-1 to the end of FP-III can be termed together as the "fusion loop" (Fig. 1A). But how these FPs in the loop can act synergistically to trigger the membrane fusion process has not been understood yet.

Spike receptor binding and fusion peptide: a structural perspective. To understand the synergy of the FPs in the trigger process, it is important to understand the structure of the Spike protein in the proper context. The FP-I to FP-III are surface exposed and are contiguous to each other in space as seen from the three-dimensional structures of the Spike fusion domain (Fig. 2, cartoon diagrams). While FP-I to FP-III are always surface exposed in the full-length, the FP-IV is deeply buried and interface the virus membrane. Therefore, while FP-I to FP-III are always available for early contacts with the host membrane, FP-IV can participate in the process post the conformational transition which may expose it for interaction with the host membrane. To understand what guarantees the FP surfaces to make the initial protein-host membrane contact, one must look at the possible modes of virus-host attachment through the Spike. For example, if three RBDs in the trimeric structure finds a host receptor, it can attain a tripod binding mode (Fig. 3A). A recent structure of the trimeric Spike complexed with a host receptor reveals the precise geometry of CEACAM1 binding the RBD of Spike from MHV-A59[35]. However, a tripod binding requires receptor molecules on the host membrane to be pre-available in a specific arrangement. High expression of receptor molecules on the host cell surface is expected to increase the probability of tripod binding, but there is no existing information whether such a precise

arrangement is present on the host surface suitable for interaction with the trimeric RBD. Moreover, the membrane bilayer structure does not contain any feature that can direct such regular host receptor arrangement. It may be noted that only in a tripod arrangement, the pre-hairpin/pre-bundle helices of the fusion domain are expected to interact head-on with the host membrane and the N-terminal segment of the S2 domain will interact early during the protein-membrane contact. In such a situation, the existing model of structural transition will follow[8]. FP-I and FP-II are located middle of the cylinder-like Spike S2 structure (Fig. 3A) and a conformational transition is needed to place them near the head of the cylinder. Here, FP1 is expected to make the early host-membrane contact if the cleavage is at the S1/S2 site and FP-II if the cleavage is at the S2' site (see Fig. 1A). The FP-III region has limited scope to make any early contact due to its farthest position from the host membrane surface. In tripod binding mode the virus membrane is still ~150Å away, and the three HR2 regions need to fold back and bind to the hydrophobic grooves of the HR1 trimer in an antiparallel manner to bridge this gap and form a hemifusion structure with the host membrane[8].

Spike fusion peptide trigger. Alternately, if only one or two RBDs bind the receptor, the vertical anchoring of the Spike fusion domain relative to the host surface is not feasible based on simple structural considerations. Also, a recent trimeric structure of SARS-CoV-2 Spike has shown a single RBD to be in open conformation[3]. In such a state, the interaction of the open RBD with the host (Fig. 3B) is not expected to stabilize the Spike anchoring in any specific orientation relative to the host due to the weak interaction with the fusion domain. Here a post-cleaved S2 domain is expected to interact side-on to the membrane surface through a "belly" landing to trigger the fusion process (Fig. 3C). It is to be noted that the shape of the trimeric S2 domain is not a proper cylinder, but with a bulge in the mid-segment which we call a "belly". The FP-II and FP-I surfaces are located at the crest of this bulge, such that it is able the make the initial contact with the host membrane. The structural constraints that guarantee the "belly" landing can be understood from the overall geometry of the Spike (Fig. 3D). The relative location of the NTD in Spike form three vertices of a triangle, while the FP-I to F-III are located midpoint of the sides, forming the vertices of an inner triangle. If the receptor attachment is in two RBD locations, the S2 landing will be close to the midpoint of the two vertices of the outer triangle coincident to the FP surfaces. Even for one-legged attachment, the contact must always be directed towards the midpoint of the two NTDs because that allows maximum contact surface to be formed where the Spike can stably rest on the host surface. During the contact, the membranotropic segment of the fusion loop spanning the FPs is expected to engage the host membrane during the fusogenic conformational change. In this case, the FP sites are proximal to the virus membrane surface such that hemifusion membrane structures can be initiated early in comparison to the tripod-binding mode which requires an intermediate pre-hairpin structure to be formed. It is also to be noted that weak RBD binding to S2 domain or disintegration of the Spike trimer post tripod binding can mimic the one- or two-legged binding mode.

SARS-CoV-2 fusion peptide distinctions. The physicochemical property of the fusion loop and the synergy of the FPs therein is critical to the rapid initiation and transition to the hemifusion stage of the membrane fusion process. The reorganization of the fusion loop and formation of the eventual six-helix bundle would have its side-face making maximum possible interface while contacting the host surface. Since the exerted force during the conformation transition is tangential to the host surface, the orthogonal frictional forces may allow an efficient scything action based

on the physiochemical nature of the contact engaged by the fusion loop. The nature of the initial surfaces of the fusion loop can be obtained from the electrostatic potential of the FP-I to FP-III surface patches[36] (Fig. 2, surface diagrams). Among the six Spike proteins considered in this study, SARS-CoV-2 has the most hydrophobic/neutral electrostatic FP patches (WHITE colored) most suitable for membrane disruption. It also has the least amount of highly negative electrostatic surface (RED colored patches) which repel the attachment of the S2 domain to the host membrane due to the repelling hydrophilic surface of the outer membrane composed of negatively charged fatty acid groups. On the other hand, a positive electrostatic surface (BLUE colored patches) may allow protein surface to tightly attach to the membrane exterior through charge attraction. The presence of an interfacial ion like the Ca^{+2} can cap the negative charge at the FP surface to assist fusion trigger - consistent with the membrane charge compatibility requirements. The disruption efficiency of surface patches is, therefore, likely to be highest for the hydrophobic/neutral, followed by the positive and negative electrostatic potential, unless modulated by an interfacial cation like the Ca^{2+}. One may argue that large patches of negative electrostatic surface potential (RED color) in the HCoV-HKU1 and HCoV-OC43 Spike fusion domain may explain the mild nature of those viruses.

Aside from the electrostatics, the physical rigidity of the fusion loop in Spike is of prime importance for the virus fusogenicity. This is because the Spike fusion domain being metastable, any local alteration of rigidity has global implications for the molecule. This has been alluded to by the mutation studies on the fusion peptide central prolines[27-30], but its criticality was recently revealed from our comprehensive studies on centrally located consecutive prolines in MHV-A59 Spike fusion peptide[6]. Proline being an imino-acid with unique structure, has restricted torsional freedom, which in turn restricts the torsional freedom of the protein backbone where it is located[37]. When two consecutive prolines are located, the rigidity of the protein backbone is further enhanced. Among the six Spike proteins in our study, three has a single central proline in FP-I, and two centrally located consecutive prolines occur in SARS-CoV-2 Spike FP-1. There are no central prolines in FP-II and a single conserved central proline in FP-IV, while consecutive prolines exist at a central location in HCoV-HKU1, HCoV-OC43, and MHV-A59 FP-III Spikes. To understand the intrinsic flexibility/rigidity of the surface exposed FPs, we set up a 500 ns molecular dynamics simulations[38] using CHARMM forcefield[39] (Fig. 4). The starting structures of all the FP-I fragments are devoid of stable secondary structures such as helices or sheets and is dominated by turns, and irregular structures indicating that the region prefers to be in a loop conformation. This is true even for the MHV-A59 Spike, which is flexible as experimentally evidenced by the lack of coordinate from the electron density map for complete FP-I in the PDB file: 3JCL. In comparison, FP-IIs in all cases are dominated by helical conformation, with the N-terminal FP segments always in a helical state. This is true for FP-III region fragments as well. Given an irregular structure, the effect of proline is more dramatic on the FP-I region in contrast to FPs from FP-II and FP-III which are already stabilized by hydrogen bonds in helices. For all FPs in the FP-I region, although local secondary structures are induced during simulation, the lowest root-mean-square fluctuation (RMSF) for a residue is achieved only by the SARS-CoV-2 consecutive proline containing FP. This can also be confirmed from the energy landscape plot created from the molecular dynamics simulation trajectory (Fig. S2) where it has the most compact single conformational well among all the FP-Is. If we look at the FP-III regions where other

consecutive proline containing FPs exist, HCoV-OC43 has the lowest RMSF; SARS-CoV-2 FP-III segment does not have any central proline, but it contains a unique "Thr-Ile-Thr" segment constituted of three consecutive β-branched side-chain residues that can impart substantial rigidity based on steric considerations[37] if not as much as the consecutive prolines. This can be again confirmed from the energy landscape plot which shows a single compact conformational well in contrast to the other FP-IIIs (Fig. S2). The observations are consistent with our previous comparative molecular dynamics studies[6] on MHV-A59 FP-III and single central proline containing FP-III from another parental non-neurotropic strain of murine hepatitis virus (MHV), MHV-2, where we found the FP-III from the former became more rigid than the latter in methanolic conditions compared to water. Additionally, NMR studies on the MHV-A59 FP-III fragment revealed its unique ability to form *cis*-peptide at the central P-P peptide bond[6]. A *cis*-trans isomerization during the membrane fusion process has the potential to expose the hydrophobic residues efficiently around the isomerized-peptide neighborhood, enhancing the fusion trigger potential. While the structural role of proline cannot be discounted, other stabilizing interactions also dominate the FPs, among which the formation of the aromatic/hydrophobic clusters is of relevance to the fusion process (see Fig. S2 for examples). As observed from the packing of the loops, a combination of aromatic and Val/Ile/Leu side chains pack tightly to exclude water. But when these regions become exposed during the conformational transition, they would enhance the hydrophobic interaction of the protein surface with the membrane. In all S2 domains, however, FP-III regions are in part masked by the FP-I segment, as evident from the relative solvent accessible surface area (SASA) values indicated in Fig. 4. The FP-III region can get fully exposed post cleavage at the S2' site which dislodges the sheathing FP-I segment, or when the site gets progressively exposed during the conformational transition amidst the fusion process.

Experimental corroboration. Additional evidence of "rigidity" imparted by proline being critical for virus fusogenicity, infectivity and pathogenicity can be obtained from our previous in vitro and in vivo studies[6]. We generated the Spike containing two consecutive prolines at 938-939 (S-MHV-A59(PP)) in the FP-III and its proline deletion (Δ938) mutant S-MHV-A59(P) from isogenic recombinant strain of MHV-A59, RSA59[6] Spike protein. The proline deleted mutant only Spike gene construct S-MHV-A59(P) show slower trafficking to the cell surface, and significantly less fusogenicity. Established on differential properties of proline deletion in Spike construct, we generated proline deleted targeted recombinant mutant strain RSA59(P-) which contains S-MHV-A59(P) and compared it with two consecutive proline-containing parental isogenic strain RSA59 containing S-MHV-A59(PP). Proline deleted mutant RSA59(P-) infection in neuronal cell line demonstrated less aggressive and fewer syncytia formation, and one order lower viral titers post-infection *in vitro*. Based on these *in vitro* differential properties of proline deletion in Spike construct we generated proline deleted targeted recombinant mutant strain of RSA59(P-) which contains S-MHV-A59(P) and compared it with two consecutive proline containing parental isogenic strain RSA59 containing S-MHV-A59(PP). The *in vivo* studies in mice parallels the *in vitro* studies demonstrating significantly reduced viral replication and consecutive disease pathologies, like less severity in meningitis, encephalitis, and demyelination, and inability to infect the retina nor induce loss of retinal ganglion cells[40]. The non-neurotropic strain MHV-2 sharing 91% genome identity with MHV-A59, and 83% pairwise Spike sequence identity, with a single central proline in FP-III, causes only meningitis and is unable to invade the brain parenchyma.

Computational studies of S2 fusion domains of S-MHV-A59(PP) and MHV-2 Spike involving molecular dynamics confirmed the former to be more rigid and containing more residues in the regular secondary structure[6].

Target for therapy. Our study brings out the importance of the fusion loop region which could be a legitimate target for the design of vaccine or synthetic agents for therapy against COVID-19. The S2 domain serves as a better therapeutic target than S1 due to higher evolutionary conservation, but the few attempts made have mainly focussed attention on the heptad repeat regions[8]. Two important features that also make the fusion loop an attractive therapeutic target are its accessibility due to its surface exposure in the full-length Spike, and the relatively high conservation of residues in the fusion loop, especially around the FP-II region which increases its scope as a pan-coronavirus target that can cater to future pandemic threats as well. Mimetic peptides can be designed to bind to the fusion loop to inhibit the fusogenic conformational transition of the S2 domain. Impairment of the fusion trigger would have a direct bearing on the fusogenicity of the virus and contribute to the reduction of lung invasion and damage that clinically results in acute pneumonia. Systematic studies can identify the minimal motif in the fusion loop serving as the fusogenic determinant to improve our selection of a potential therapeutic target to prevent cell-to-cell fusion and subsequent pathogenesis.

Discussion and conclusions. The interplay of the outlined physicochemical features determines the virus-entry process to become more efficient. The local and global stability of the S2 domain is important. Since the S2 domain undergoes a conformational transition, local stability means reasonably rigid moving parts, and global stability means a well-defined conformational transition pathway from the metastable to the stable state. This local and global stability requirement could be attributed to the physicochemical efficiency needed in disturbing the host membrane. Secondly, the electrostatic potential of the fusion peptide derived surface patches must be neutral or positive to be able to engage the host membrane. The presence of glycosylation sites adds to the hydrophobicity of the S2 domain surface, but it is a small fraction of the available surface for interaction with the host membrane. The fusogenic conformational transition requires optimal synergy between the physical and chemical properties of the fusion loop to allow a concurrent scything action to rapidly facilitate transition to the host-virus hemifusion membrane state. The free-energy available from the conformational transition of S2 to a more relaxed helical bundle is available to disrupt the host membrane and overcome the kinetic barrier to bring the host and virus membrane lipid bilayers together. The pre-hairpin S2 intermediate as suggested to exist by many researchers may be one of the many conformational states interacting with the host membrane. Priming by Spike cleavage is important for facilitating the fusion process and therefore a part of the synergy at play. However, the open conformation of RBD seen in PDB ID: 6VSB for SARS-CoV-2 suggests that flexible linker segments loosely connect the RBD back to the fusion domain leaving it relatively free for unfettered conformational transition. Therefore, multifarious options to prime and trigger appear to be available to SARS-CoV-2 for viral entry, which contributes to its increased infectivity. Preventing the trigger by inhibiting the fusion loop is therefore a suitable target for therapy. Given the importance, a more extensive study of SARS-CoV-2 Spike protein and the mechanistic hypothesis described here is therefore warranted.

Online Methods

The sequences used in this study were downloaded from the NCBI database (URL:http://www.ncbi.nlm.nih.gov). The multiple sequence alignments were performed using the T-coffee webserver (http://tcoffee.crg.cat/). The default parameter values for alignment available in the server were used. The server combines several methods to come up with an optimal multiple sequence alignment[9].

All protein three-dimensional structures were downloaded from the Protein Data Bank (http:/www.rcsb.org). The PDB IDs for the downloaded structures are HCoV-HKU1: 5I08, MHV-A59: 3JCL, 6VSJ, HCoV-OC43: 6NZK, MERS-CoV: 6Q04, SARS-CoV-2: 6VXX, 6VSB, and SARS-CoV: 5XLR. Structures with the highest resolution was preferred when more than one model was available. Coordinates from these files were extracted for obtaining starting models of the FPs used in our molecular dynamics simulations. Whenever there were missing coordinates, they were modeled as an extended structure in the FP. The SASA was calculated by the program NACESS (http://wolf.bms.umist.ac.uk/naccess/); residues for which no atom coordinates are present in the PDB file was considered as fully exposed to solvent while calculating the relative SASA values. The secondary structure was calculated by the SECSTR program from the PROCHECK suite (https://www.ebi.ac.uk/thornton-srv/software/PROCHECK/). The electrostatic surface potential was calculated using the APBS plugin[36] inside the PyMol software (http://pymol.org). The default parameters were used for the calculations. All cartoon diagrams and surfaces were rendered by the PyMol software.

The molecular dynamics simulations were performed with GROMACS software[38] (http://www.gromacs.org). The simulations were performed using the CHARMM 27 forcefield with cmap[39]. Each FP was placed in a cubic box solvated with water (SPC model). Solvent molecules were randomly replaced with Na^+ and Cl^- to neutralize the system and bring the final concentration of NaCl to 0.1 M. Periodic boundary conditions were enforced in all three directions. The system was minimized until the maximum force in the system reached below 1000 kJ mol^{-1} nm^{-1}. The systems were equilibrated for 2 ns under the NVT ensemble. This was followed by equilibration for 2 ns in the NPT ensemble at 1 atm and 300 K. The production run was executed for 500 ns saving the output every 100 ps yielding 5,000 frames for analysis. The analysis of the trajectory was performed using GROMACS utilities. The diagrams were created using our in-house software.

Acknowledgment

DP thanks the Department of Biotechnology, New Delhi for supporting the computational facilities, and Prof. Jayasri Das Sarma, Department of Biological Sciences, Indian Institute of Science Education and Research Kolkata for her generous support.

Conflict of Interest

The author has no conflict of interest.

Materials and Correspondence

All requests may be forwarded to DP.

References

1 Zheng, J. SARS-CoV-2: an Emerging Coronavirus that Causes a Global Threat. *Int J Biol Sci* **16**, 1678-1685, DOI:10.7150/ijbs.45053 (2020).

2 Li, F. Structure, Function, and Evolution of Coronavirus Spike Proteins. *Annual Review of Virology* **3**, 237-261, DOI:10.1146/annurev-virology-110615-042301 (2016).

3 Wrapp, D. *et al.* Cryo-EM structure of the 2019-nCoV spike in the prefusion conformation. *Science* **367**, 1260-1263 (2020).

4 Tai, W. *et al.* Characterization of the receptor-binding domain (RBD) of 2019 novel coronavirus: implication for development of RBD protein as a viral attachment inhibitor and vaccine. *Cellular & Molecular Immunology*, DOI:10.1038/s41423-020-0400-4 (2020).

5 Hoffmann, M. *et al.* SARS-CoV-2 cell entry depends on ACE2 and TMPRSS2 and is blocked by a clinically proven protease inhibitor. *Cell* (2020).

6 Singh, M. *et al.* A proline insertion-deletion in the spike glycoprotein fusion peptide of mouse hepatitis virus strongly alters neuropathology. *J Biol Chem* **294**, 8064-8087, DOI:10.1074/jbc.RA118.004418 (2019).

7 Shi, Y. *et al.* COVID-19 infection: the perspectives on immune responses. *Cell Death & Differentiation* **27**, 1451-1452 (2020).

8 Tang, T., Bidon, M., Jaimes, J. A., Whittaker, G. R. & Daniel, S. Coronavirus membrane fusion mechanism offers as a potential target for antiviral development. *Antiviral Research*, 104792 (2020).

9 Di Tommaso, P. *et al.* T-Coffee: a web server for the multiple sequence alignment of protein and RNA sequences using structural information and homology extension. *Nucleic acids research* **39**, W13-W17 (2011).

10 Sadasivan, J., Singh, M. & Sarma, J. D. Cytoplasmic tail of coronavirus spike protein has intracellular targeting signals. *J Biosci* **42**, 231-244, DOI:10.1007/s12038-017-9676-7 (2017).

11 Das Sarma, J. *et al.* Demyelinating and nondemyelinating strains of mouse hepatitis virus differ in their neural cell tropism. *Journal of virology* **82**, 5519-5526, DOI:10.1128/JVI.01488-07 (2008).

12 Das Sarma, J., Kenyon, L. C., Hingley, S. T. & Shindler, K. S. Mechanisms of primary axonal damage in a viral model of multiple sclerosis. *J Neurosci* **29**, 10272-10280, DOI:10.1523/JNEUROSCI.1975-09.2009 (2009).

13 Das Sarma, J., Scheen, E., Seo, S. H., Koval, M. & Weiss, S. R. Enhanced green fluorescent protein expression may be used to monitor murine coronavirus spread in vitro and in the mouse central nervous system. *Journal of neurovirology* **8**, 381-391, DOI:10.1080/13550280260422686 (2002).

14 Kenyon, L. C. *et al.* Gliopathy of Demyelinating and Non-Demyelinating Strains of Mouse Hepatitis Virus. *Front Cell Neurosci* **9**, 488, DOI:10.3389/fncel.2015.00488 (2015).

15 Walls, A. C. *et al.* Structure, function, and antigenicity of the SARS-CoV-2 spike glycoprotein. *Cell* **181**, 281-292 (2020).

16 Marzi, A. *et al.* DC-SIGN and DC-SIGNR interact with the glycoprotein of Marburg virus and the S protein of severe acute respiratory syndrome coronavirus. *Journal of virology* **78**, 12090-12095, DOI:10.1128/JVI.78.21.12090-12095.2004 (2004).

17 Vaduganathan, M. *et al.* Renin–Angiotensin–Aldosterone System Inhibitors in Patients with Covid-19. *New England Journal of Medicine*, DOI:10.1056/NEJMsr2005760 (2020).

18 Belouzard, S., Madu, I. & Whittaker, G. R. Elastase-mediated activation of the severe acute respiratory syndrome coronavirus spike protein at discrete sites within the S2 domain. *The Journal of biological chemistry* **285**, 22758-22763, DOI:10.1074/jbc.M110.103275 (2010).
19 Hingley, S. T., Leparc-Goffart, I., Seo, S. H., Tsai, J. C. & Weiss, S. R. The virulence of mouse hepatitis virus strain A59 is not dependent on efficient spike protein cleavage and cell-to-cell fusion. *Journal of neurovirology* **8**, 400-410, DOI:10.1080/13550280260422703 (2002).
20 Broer, R., Boson, B., Spaan, W., Cosset, F.-L. & Corver, J. Important role for the transmembrane domain of severe acute respiratory syndrome coronavirus spike protein during entry. *Journal of virology* **80**, 1302-1310 (2006).
21 Petit, C. M. *et al.* Genetic analysis of the SARS-coronavirus spike glycoprotein functional domains involved in cell-surface expression and cell-to-cell fusion. *Virology* **341**, 215-230 (2005).
22 Alsaadi, E. A. J., Neuman, B. W. & Jones, I. M. A Fusion Peptide in the Spike Protein of MERS Coronavirus. *Viruses* **11**, DOI:10.3390/v11090825 (2019).
23 Guillen, J., Kinnunen, P. K. & Villalain, J. Membrane insertion of the three main membranotropic sequences from SARS-CoV S2 glycoprotein. *Biochim Biophys Acta* **1778**, 2765-2774, DOI:10.1016/j.bbamem.2008.07.021 (2008).
24 Guillen, J., Perez-Berna, A. J., Moreno, M. R. & Villalain, J. A second SARS-CoV S2 glycoprotein internal membrane-active peptide. Biophysical characterization and membrane interaction. *Biochemistry* **47**, 8214-8224, DOI:10.1021/bi800814q (2008).
25 Sainz, B., Jr., Rausch, J. M., Gallaher, W. R., Garry, R. F. & Wimley, W. C. Identification and characterization of the putative fusion peptide of the severe acute respiratory syndrome-associated coronavirus spike protein. *Journal of virology* **79**, 7195-7206, DOI:10.1128/JVI.79.11.7195-7206.2005 (2005).
26 White, J. M. Viral and cellular membrane fusion proteins. *Annu Rev Physiol* **52**, 675-697, DOI:10.1146/annurev.ph.52.030190.003331 (1990).
27 Delos, S., Gilbert, J. & White, J. The central proline of an internal viral fusion peptide serves two important roles. *Journal of virology* **74**, 1686-1693 (2000).
28 Gómara, M. a. J., Mora, P., Mingarro, I. & Nieva, J. L. Roles of a conserved proline in the internal fusion peptide of Ebola glycoprotein. *FEBS Letters* **569**, 261-266 (2004).
29 Fredericksen, B. L. & Whitt, M. A. Vesicular stomatitis virus glycoprotein mutations that affect membrane fusion activity and abolish virus infectivity. *Journal of virology* **69**, 1435-1443 (1995).
30 Drummer, H. E. & Poumbourios, P. Hepatitis C virus glycoprotein E2 contains a membrane-proximal heptad repeat sequence that is essential for E1E2 glycoprotein heterodimerization and viral entry. *Journal of Biological Chemistry* **279**, 30066-30072 (2004).
31 Harrison, S. C. Viral membrane fusion. *Nature structural & molecular biology* **15**, 690-698 (2008).
32 Xia, S. *et al.* Inhibition of SARS-CoV-2 (previously 2019-nCoV) infection by a highly potent pan-coronavirus fusion inhibitor targeting its spike protein that harbors a high capacity to mediate membrane fusion. *Cell research*, 1-13 (2020).
33 Ou, X. *et al.* Identification of the fusion peptide-containing region in betacoronavirus spike glycoproteins. *Journal of virology* **90**, 5586-5600 (2016).

34 Wimley, W. C. & White, S. H. Experimentally determined hydrophobicity scale for proteins at membrane interfaces. *Nat Struct Biol* **3**, 842-848, DOI:10.1038/nsb1096-842 (1996).
35 Shang, J. *et al.* Structure of mouse coronavirus spike protein complexed with receptor reveals mechanism for viral entry. *PLoS pathogens* **16**, e1008392 (2020).
36 Jurrus, E. *et al.* Improvements to the APBS biomolecular solvation software suite. *Protein Science* **27**, 112-128 (2018).
37 Chakrabarti, P. & Pal, D. The interrelationships of side-chain and main-chain conformations in proteins. *Progress in biophysics and molecular biology* **76**, 1-102 (2001).
38 Abraham, M. J. *et al*. GROMACS: High performance molecular simulations through multi-level parallelism from laptops to supercomputers. *SoftwareX* **1**, 19-25 (2015).
39 Bjelkmar, P., Larsson, P., Cuendet, M. A., Hess, B. & Lindahl, E. Implementation of the CHARMM Force Field in GROMACS: Analysis of Protein Stability Effects from Correction Maps, Virtual Interaction Sites, and Water Models. *Journal of Chemical Theory and Computation* **6**, 459–466 (2010).
40 Rout, S. S., Singh, M., Shindler, K. S. & Das Sarma, J. One proline deletion in the fusion peptide of neurotropic mouse hepatitis virus (MHV) restricts retrograde axonal transport and neurodegeneration. *J Biol Chem*, DOI:10.1074/jbc.RA119.011918 (2020).

Figure Legend

Fig. 1. The S2 domain organization of SARS-CoV-2 Spike glycoprotein and its sequence comparison against seven other coronaviruses. (A) The denomination of the various S2 domain segments and their positions. The labels are as follows, FL: Fusion Loop, HR1: Hepatad Repeat 1, CH: Central Helix, CD: Connector Domain, HR2: Heptad Repeat 2, TM: Transmembrane Domain, CP: Cytoplasmic tail. The span of the segments can be estimated from the position markers indicated for SAR-CoV-2 (SARS2) and SARS-CoV (SARS). (B) Multiple sequence alignment (MSA) of the S2 domain of Spike protein from eight coronaviruses. The segments of the S2 domain are also marked by position markers. Residues underlined in the MSA have no coordinates in the structure file and are deemed flexible regions. The PDB files used to mark the same are SARS-CoV-2: 6VXX, SARS-CoV:5XLR, MERS-CoV: 6Q04, MHV-A59: 3JCL, HCoV-OC43: 6NZK, HCoV-HKU1: 5I08. The sequences for HCoV-NL63 and HCoV-2289E are not marked because they belong to α-coronaviruses; whereas, all others are from β-coronaviruses. The RED marked region spanning Heptad repeat region 2 C-terminal and trans-membrane domain N-terminal region is also called the aromatic domain or the FP-IV. The MSA of the full-length protein can be found in Fig. S1.

Fig. 2. Cartoon diagram showing the fusion peptide regions FP-I (orange), FP-II (green), and FP-III (dark grey) on the trimeric fusion domain structure of Spike from six viruses. The electrostatic surface of the fusion domain is shown adjacent to each structure and the corresponding fusion peptide regions are marked by an arrow. The orientation of the cartoon structure and the electrostatic surface are aligned among themselves. Note that one face of the electrostatic surface that is visible is repeated on the other side due to the symmetry arising out of the trimeric quaternary structure. The fusion domain structures are shown in cyan for helices, strands in red, and loops in magenta. Please refer to Fig. 1 for the sequence alignment and its legend for the PDB ID of files used to draw the structures. Note that a part of the FP-I surface is absent for MHV-A59 and HCoV-HKU1 due to unavailable atom coordinates in the PDB file. The same is true for a small section of FP-II from SARS-CoV-2. For residue details, please refer to Fig. 4. All FP-I regions have at least one Asn-linked site, only SARS-CoV-2, SARS-CoV, and HCoV-HKU1 has a site in FP-II, and HCoV-OC43 and HCoV-HKU1 in FP-III. Contiguous to the FP-III are the heptad repeat regions where the glycosylation and sequence conservation among Spike is the highest. Spike from MHV-A59 shares a 64-66% overall sequence identity with HCoV-HKU1 and OC43, 71-76% identity with the corresponding S2 domains. Similar match with SARS-CoV, MERS-CoV, and SARS-CoV-2 are at <30% pairwise sequence identity.

Fig. 3. **Schematic diagrams explaining the mode of binding of Spike protein to the host receptor and its putative orientation relative to the host membrane surface during the virus-host attachment.** (A). A cartoon diagram created using PDB ID: 6VSJ where the Spike protein from MHV-A59 is in complex with CEACAM1 receptor from mouse. Since all three subunits from the Spike RBD attach to the receptor, it allows the virus to anchor in a tripod mode. The approximate length of the Spike in the longer dimension is indicated along with the FP locations. (B). A cartoon diagram created using PDB ID: 6VSB, where one of the RBDs are shown in an open conformation. A receptor molecule ACE2 has been drawn to show the putative attachment in one-legged mode. Two-legged mode may also be possible similarly. (C). The S2 domain of

SARS-CoV-2 Spike protein is shown in a belly-landing orientation. The approximate length of the Spike in the longer dimension is indicated along with the marked FP locations. (D) A ribbon diagram of the trimeric Spike proteins from the six coronaviruses used in this study. Two triangles are marked on each structure, where the relative locations of the protruding NTDs appear near the outer triangle vertices, and the FP-I, FP-II, and FP-III colored surfaces are located near the inner triangle vertices. The triangles are marked to bring out the relative positions of the NTDs and the FP surfaces. The Spike structure is oriented such that the RBD appears closest to the eye, followed by the NTD and then the FPs.

Fig. 4. **Graphs showing various parameters calculated from the simulation trajectory of the isolated fragments from FP-I, FP-II, and FP-III of six coronaviruses.** The bar diagrams are drawn showing the secondary structure prevalence in 500 ns simulation, overlaid by the curves for Solvent Accessible Solvent Area (SASA; $Å^2$), and Root-Mean-Square-Fluctuation (RMSF; Å). The Y-axis scales provide values for SASA and RMSF side-by-side. The standard deviation of the SASA in the simulation is indicated by a shaded background around the SASA curve. The X-axis indicates the residues for each FP fragment. The central proline residues are marked in BOLD and those residues for which the atom coordinates are absent in the PDB file are marked in RED. Below the residues, the corresponding secondary structures as indicated as present in the full-length protein. The symbols mean as follows, H:α-helix, h: α-helix termini, G: 3_{10}-helix, g: 3_{10}-helix termini, B: β-bridge, E: β-strand, e: β-strand termini, T: hydrogen-bonded turn, t: hydrogen-bonded turn termini, S: Bend, and <space>: irregular secondary structure. The first, second, and third columns are indicated by Labels I, II, and III corresponding to FP-I, FP-II, and FP-III in each Spike protein from a given virus, respectively. The relative SASA value of the whole FP fragment in the S2 domain expressed as a percentage is indicated in BOLD on the top part of each plot.

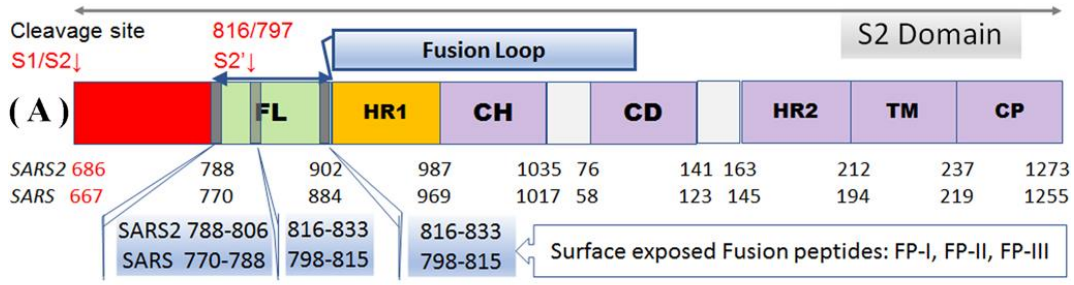

(B) Multiple Sequence Alignment

BAD AVG GOOD

FC:Furin Cleavage Site (S1/S2 domain boundary)[1]:RXXR↓

```
SARS2|QIK02964.     PTWRVYSTGSNVFQTR--AGCLIGAEHVNN--SYECDIPIGAGICASYQTQT-NSPRRARSVA 688
SARS|NP_828851.     PAWRIYSTGNNVFQTQ--AGCLIGAEHVDT--SYECDIPIGAGICASYHTVS-L-LR---STS 670
MERS|QBM11748.1     SMLKRRDSTYGPLQTP--VGCVLGLVNSSL-FVEDCKLPLGQSLCALPDTPSTLTPRSVRSVP 754
MHV-A59|AAU0635     --------PLNYFDSY--LGCVVNADNRTDEALPNCDLRMGAGLCVDYSKS----RRAHRSVS 720
OC43|YP_0095552     --------PINYFDSY--LGCVVNAYNSTAISVQTCDLTVGSGYCVDYSKN----RRSRGAIT 761
HKU1|Q14EB0.1       --------P-FYFDSY--LGCVLNAVNLTSYSVSSCDLRMGSGFCIDYALPS-S-RRKRRGIS 759
NL63|YP_003767.     --------PNFYYVSNGGNNCTTA-----------VMTYSNFGICADGSLIP-VRPRNSS--- 751
228E|NP_073551.     --------PKFFYASNGTYNCTDA-----------VLTYSSFGVCADGSIIA-VQPRNVS--- 570
Consensus                      :   .*                      . . *                *

SARS2|QIK02964.     SQSI----IAYTMSLGAENSVAY-SNNSIAIPTNFTISVTTEILPVSMTKTSVDCTMYICGDS 746
SARS|NP_828851.     QKSI----VAYTMSLGADSSIAY-SNNTIAIPTNFSISITTEVMPVSMAKTSVDCNMYICGDS 728
MERS|QBM11748.1     GEMRLAS-IAFNHPIQVDQLNS--SYFKLSIPTNFSFGVTQEYIQTTIQKVTVDCKQYVCNGF 814
MHV-A59|AAU0635     TGYRLTTFEPYTPMLVNDSVQSVDGLYEMQIPTNFTIGHHEEFIQTRSPKVTIDCAAFVCGDN 783
OC43|YP_0095552     TGYRFTNFEPFTVNSVNDSLEPVGGLYEIQIPSEFTIGNMVEFIQTSSPKVTIDCAAFVCGDY 824
HKU1|Q14EB0.1       SPYRFVTFEPFNVSFVNDSVETVGGLFEIQIPTNFTIAGHEEFIQTSSPKVTIDCSAFVCSNY 822
NL63|YP_003767.     ----------------DNGISAI-ITANLSIPSNWTTSVQVEYLQITSTPIVVDCATYVCNGN 797
228E|NP_073551.     ----------------YDSVSAI-VTANLSIPSNWTTSVQVEYLQITSTPIVVDCSTYVCNGN 616
Consensus                        :   .      : **:::: .   * :         :**  ::*..
```

← Fusion Peptide I[3]

```
SARS2|QIK02964.     TECSNLLLQYGSFCTQLNRALTGIAVEQDKNTQEVFAQVKQIYKT-PPI-----KDFG-GFNF 802
SARS|NP_828851.     TECANLLLQYGSFCTQLNRALSGIAAEQDRNTREVFAQVKQMYKT-PTL-----KYFG-GFNF 784
MERS|QBM11748.1     QKCEQLLREYGQFCSKINQALHGANLRQDDSVRNLFESVKSSQSS-PII-----PGFGGDFNL 871
MHV-A59|AAU0635     TACRQQLVEYGSFCVNVNAILNEVNNLLDNMQLQVASALMQGVTISSRLPDGISGPID-DINF 845
OC43|YP_0095552     AACKSQLVEYGSFCDNINAILTEVNELLDTTQLQVANSLMNGVTLSTKLKDGVNFNVD-DINF 886
HKU1|Q14EB0.1       AACHDLLSEYGTFCDNINSILNEVNDLLDITQLQVANALMQGVTLSSNLNTNLHSDVD-NIDF 884
NL63|YP_003767.     PRCKNLLKQYTSACKTIEDALRLSAHLETNDVSSMLTFDSNAFSL-ANV-----TSFG-DYNL 853
228E|NP_073551.     VRCVELLKQYTSACKTIEDALRNSARLESADVSEMLTFDKKAFTL-ANV-----SSFG-DYNL 672
Consensus             * . * :*   *  ::  *                .:     .  .  . :      ..  . ::
```

→ S2'↓← Fusion Peptide II[1] →

```
SARS2|QIK02964.     SQILPD-----------PSKPSKRSFIEDLLFNKVTLADAGFIKQ-YGDCL--GDIAARDLIC 851
SARS|NP_828851.     SQILPD-----------PLKPTKRSFIEDLLFNKVTLADAGFMKQ-YGECL--GDINARDLIC 833
MERS|QBM11748.1     TLLEPVSIST-------GS-RSARSAIEDLLFDKVTIADPGYMQG-YDDCMQQGPASARDLIC 925
MHV-A59|AAU0635     SPLLGCIGSTCAEDGNGPSAIRGRSAIEDLLFDKVKLSDVGFVEA-YNNCT--GGQEVRDLLC 905
OC43|YP_0095552     SPVLGCLGSEC-------SKASSRSAIEDLLFDKVKLSDVGFVEA-YNNCT--GGAEIRDLIC 939
HKU1|Q14EB0.1       KSLLGCLGSQC--------GSSSRSLLEDLLFNKVKLSDVGFVEA-YNNCT--GGSEIRDLLC 936
NL63|YP_003767.     SSVLPQRNIR-------SSRIAGRSALEDLLFSKVVTSGLGTVDVDYKSCT--KGLSIADLAC 907
228E|NP_073551.     SSVIPSLPTS-------GSRVAGRSAIEDILFSKLVTSGLGTVDADYKKCT--KGLSIADLAC 726
Consensus           . :                   ** :**:**.*:   :. * :.   * .*          ** *
```

← Fusion Peptide III[4] → ←Heptad

```
SARS2|QIK02964.     AQKFNGLTVLPPLLTDEMIAQYTSALLAGTITSGWTFGAGAALQIPFAMQMAYRFNGIGVTQN 914
SARS|NP_828851.     AQKFNGLTVLPPLLTDDMIAAYTAALVSGTATAGWTFGAGAALQIPFAMQMAYRFNGIGVTQN 896
MERS|QBM11748.1     AQYVAGYKVLPPLMDVNMEAAYTSSLLGSIAGVGWTAGLSSFAAIPFAQSIFYRLNGVGITQQ 988
MHV-A59|AAU0635     VQSFNGIKVLPPVLSESQISGYTTGATAAAMFPPWS----AAAGVPFSLSVQYRINGLGVTMN 964
OC43|YP_0095552     VQSYKGIKVLPPLLSENQISGYTLAATSASLFPPWT----AAAGVPFYLNVQYRINGLGVTMD 998
HKU1|Q14EB0.1       VQSFNGIKVLPPILSETQISGYTTAATVAAMFPPWS----AAAGVPFSLNVQYRINGLGVTMD 995
NL63|YP_003767.     AQYYNGIMVLPGVADAERMAMYTGSLIGGMVLGGLT----SAAAIPFSLALQARLNYVALQTD 966
228E|NP_073551.     AQYYNGIMVLPGVADAERMAMYTGSLIGGIALGGLT----SAVSIPFSLAIQARLNYVALQTD 785
Consensus           .*   *  *** :       : ** .   .      :    :   :**   :  *:* :.:  :
```

```
                    Repeat Region 1 Begin[1]
SARS2|QIK02964.     VLYENQKLIANQFNSAIGKIQDSLSSTA--------------SALGKLQDVVNQNAQALNTLV 963
SARS|NP_828851.     VLYENQKQIANQFNKAISQIQESLTTTS--------------TALGKLQDVVNQNAQALNTLV 945
MERS|QBM11748.1     VLSENQKLIANKFNQALGAMQTGFTTTN--------------EAFQKVQDAVNNNAQALSKLA 1037
MHV-A59|AAU0635     VLSENQKMIASAFNNALGAIQDGFDATN--------------SALGKIQSVVNANAEALNNLL 1013
OC43|YP_0095552     VLSQNQKLIANAFNNALYAIQEGFDATN--------------SALVKIQAVVNANAEALNNLL 1047
HKU1|Q14EB0.1       VLNKNQKLIANAFNKALLSIQNGFTATN--------------SALAKIQSVVNANAQALNSLL 1044
NL63|YP_003767.     VLQENQKILAASFNKAINNIVASFSSVNDAITQTAEAIHTVTIALNKIQDVVNQQGSALNHLT 1029
228E|NP_073551.     VLQENQKILAASFNKAMTNIVDAFTGVNDAITQTSQALQTVATALNKIQDVVNQQGNSLNHLT 848
Consensus           ** :*** :*  **.*:  :  .:  .                 *: *:* .** :..:*. *
                    Heptad Repeat Region 1 End→←Central Helix Begin[1]                Central
SARS2|QIK02964.     KQLSSNFGAISSVLNDILSRLDKVEAEVQIDRLITGRLQSLQTYVTQQLIRAAEIRASANLAA 1026
SARS|NP_828851.     KQLSSNFGAISSVLNDILSRLDKVEAEVQIDRLITGRLQSLQTYVTQQLIRAAEIRASANLAA 1008
MERS|QBM11748.1     SELSNTFGAISASIGDIIQRLDVLEQDAQIDRLINGRLTTLNAFVAQQLVRSESAALSAQLAK 1100
MHV-A59|AAU0635     NQLSNRFGAISASLQEILTRLEAVEAKAQIDRLINGRLTALNAYISKQLSDSTLIKVSAAQAI 1076
OC43|YP_0095552     QQLSNRFGAISASLQEILSRLDALEAEAQIDRLINGRLTALNAYVSQQLSDSTLVKFSAAQAM 1110
HKU1|Q14EB0.1       QQLFNKFGAISSSLQEILSRLDNLEAQVQIDRLINGRLTALNAYVSQQLSDITLIKAGASRAI 1107
NL63|YP_003767.     SQLRHNFQAISNSIQAIYDRLDSIQADQQVDRLITGRLAALNAFVSQVLNKYTEVRGSRRLAQ 1092
228E|NP_073551.     SQLRQNFQAISSSIQAIYDRLDTIQADQQVDRLITGRLAALNVFVSHTLTKYTEVRASRQLAQ 911
Consensus           .:*   * ***  :  *  **: :: . *:****.*** :*:.:::: *        .   *
                    Helix End→                                        ←Connector
SARS2|QIK02964.     TKMSECVLGQSKRVDFCGKGYHLMSFPQSAPHGVVFLHVTYVPAQEKNFTTAPAICHDGK--- 1086
SARS|NP_828851.     TKMSECVLGQSKRVDFCGKGYHLMSFPQAAPHGVVFLHVTYVPSQERNFTTAPAICHEGK--- 1068
MERS|QBM11748.1     DKVNECVKAQSKRSGFCGQGTHIVSFVVNAPNGLYFMHVGYYPSNHIEVVSAYGLCDSANPTN 1163
MHV-A59|AAU0635     EKVNECVKSQTTRINFCGNGNHILSLVQNAPYGLYFIHFSYVPISFTTANVSPGLCISGDR-- 1137
OC43|YP_0095552     EKVNECVKSQSSRINFCGNGNHIISLVQNAPYGLYFIHFSYVPTKYVTARVSPGLCIAGDR-- 1171
HKU1|Q14EB0.1       EKVNECVKSQSPRINFCGNGNHILSLVQNAPYGLLFIHFSYKPTSFKTVLVSPGLCLSGDR-- 1168
NL63|YP_003767.     QKINECVKSQSNRYGFCGNGTHIFSIVNSAPDGLLFLHTVLLPTDYKNVKAWSGICVDGIY-- 1153
228E|NP_073551.     QKVNECVKSQSKRYGFCGNGTHIFSIVNAAPEGLVFLHTVLLPTQYKDVEAWSGLCVDGTN-- 972
Consensus            *:.*** .*: * .***:* *:.*:   ** *: *:*    * .         .:*  .
                     Domain Begin[1]                          Connector Domain End→
SARS2|QIK02964.     AHFPREGVFV--SNGT-----HWFVTQRNFYEPQIITTDNTFVSGNCDVVIGIVNNTVYDPLQ 1142
SARS|NP_828851.     AYFPREGVFV--FNGT-----SWFITQRNFFSPQIITTDNTFVSGNCDVVIGIINNTVYDPLQ 1124
MERS|QBM11748.1     CIAPVNGYFI--KTNNTRIVDEWSYTGSSFYAPEPITSLNTKYV-APQVTYQNISTNLPPPLL 1223
MHV-A59|AAU0635     GLAPKAGYFV--QDDG-----EWKFTGSSYYYPEPITDKNSVIMSSCAVNYTKAPEVFLNTSI 1193
OC43|YP_0095552     GIAPKSGYFV--NVNN-----TWMYTGSGYYYPEPITENNVVVMSTCAVNYTKAPYVMLNTSI 1227
NL63|YP_003767.     GYVLRQPNLVLYSDNG-----VFRVTSRVMFQPRLPVLSDFVQIYNCNVTFVNISRVELHTVI 1211
228E|NP_073551.     GYVLRQPNLALYKEGN-----YYRITSRIMFEPRIPTMADFVQIENCNVTFVNISRSELQTIV 1030
Consensus                  :    .   ▮▮▮▮▮  :  *    : *.     :          *
                                                ←Heptad Repeat Region 2[3]
SARS2|QIK02964.     PE--LDSFKEELDKY-FKNHT-SPDVDLG-DISGINASVVNIQKEID--------------RL 1186
SARS|NP_828851.     PE--LDSFKEELDKY-FKNHT-SPDVDLG-DISGINASVVNIQKEID--------------RL 1168
MERS|QBM11748.1     GNSTGIDFQDELDEF-FKNVS-TSIPNFG-SLTQINTTLLDLTYEML--------------SL 1269
MHV-A59|AAU0635     PN--PPDFKEELDKW-FKNQT-SIAPDLSLDFEKLNVTLLDLTYEMN--------------RI 1238
OC43|YP_0095552     PN--LPDFKEELDQW-FKNQT-SVAPDLS--LDYINVTFLDLQVEMN--------------RL 1270
HKU1|Q14EB0.1       PN--LSDFEAEFSLW-FKNHT-SIAPNLTF-NSHINATFLDLYYEMN--------------VI 1268
NL63|YP_003767.     PD--YVDVNKTLQEF-AQNLPKYVKPNF--DLTPFNLTYLNLSSELKQLEAKTASLFQTTVEL 1269
228E|NP_073551.     PE--YIDVNKTLQELSYKL-PNYTVPDL--VVEQYNQTILNLTSEISTLENKSAELNYTVQKL 1088
Consensus            :▮▮  ..:  :.  ▮  :  .    ::  ▮ ▮  * : :::  *:                 :
                     Heptad Repeat Region 2 End→←Transmembrane Domain[3]→←  Cytoplasmic tail
SARS2|QIK02964.     NEVAKNLNESLIDLQELGKYEQYIKWPWYIWLGFIAGLIAIVMVTIMLCCMTSCCSC---LKG 1246
SARS|NP_828851.     NEVAKNLNESLIDLQELGKYEQYIKWPWYVWLGFIAGLIAIVMVTILLCCMTSCCSC---LKG 1228
MERS|QBM11748.1     QQVVKALNESYIDLKELGNYTYYNKWPWYIWLSFIAGLVALALCVFFILCCTGCGTN--CMG- 1329
MHV-A59|AAU0635     QDAIKKLNESYINLKEVGTYEMYVKWPWYVWLLIGLAGVAVCVLLFFICCCTGCGSC--CFK- 1298
OC43|YP_0095552     QEAIKVLNQSYINLKDIGTYEYYVKWPWYVWLLICLAGVAMLVLLFFICCCTGCGTS--CFK- 1330
HKU1|Q14EB0.1       QESIKSLNSSFINLKEIGTYEMYVKWPWYIWLLIVILFIIFLMILFFICCCTGCGSA--CFS- 1328
NL63|YP_003767.     QGLIDQINSTYVDLKLLNRFENYIKWPWWVWLIISVVFVVLLSLLVFCCLSTGCCGCCNCLT- 1331
228E|NP_073551.     QTLIDNINSTLVDLKWLNRVETYIKWPWWVWLCISVVLIFVVSMLLLCCCSTGCCGFFSCFA- 1150
Consensus           :   . :*.: ::*: :.    * ****::** :    : .    .:    *.*    ▮▮ :
                    ER or ERGIC localization signal[5]:←  →
SARS2|QIK02964.     CCSCGSCCKFD--EDDSEP-VLKGVKLHYT 1273
SARS|NP_828851.     ACSCGSCCKFD--EDDSEP-VLKGVKLHYT 1255
MERS|QBM11748.1     KLKCNRCCDRY--EEYDLE--PH--KVHVH 1353
MHV-A59|AAU0635     --KCGNCCDEY--GGHQDSIVIHNISSHED 1324
OC43|YP_0095552     --KCGGCCDDY--TGYQE-LVIK--TSHDD 1353
HKU1|Q14EB0.1       --KCHNCCDEY--GGHND-FVIK--ASHDD 1351
NL63|YP_003767.     -SSMRGCCDCGSTKLPYYE--FE--KVHVQ 1356
228E|NP_073551.     -SSIRGCCEST--KLPYYD--VE--KIHIQ 1173
Consensus           ▮  .   **.  ▮▮▮▮▮▮▮▮▮▮  .
```

Fig. 1.

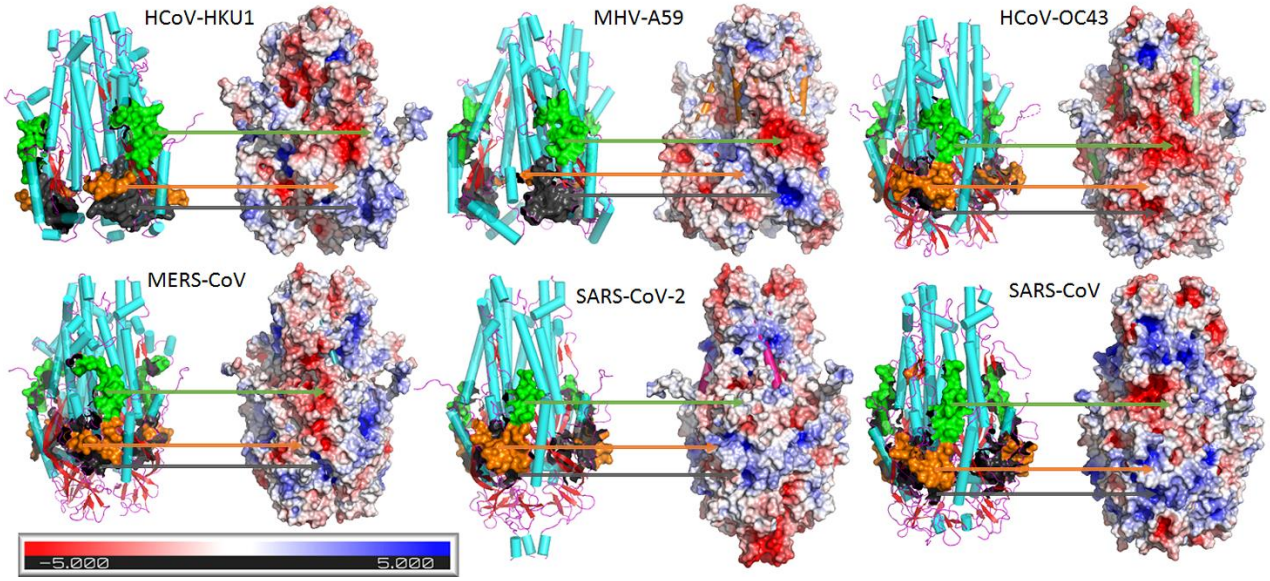
HCoV-HKU1
MHV-A59
HCoV-OC43
MERS-CoV
SARS-CoV-2
SARS-CoV
−5.000
5.000

Fig. 2.

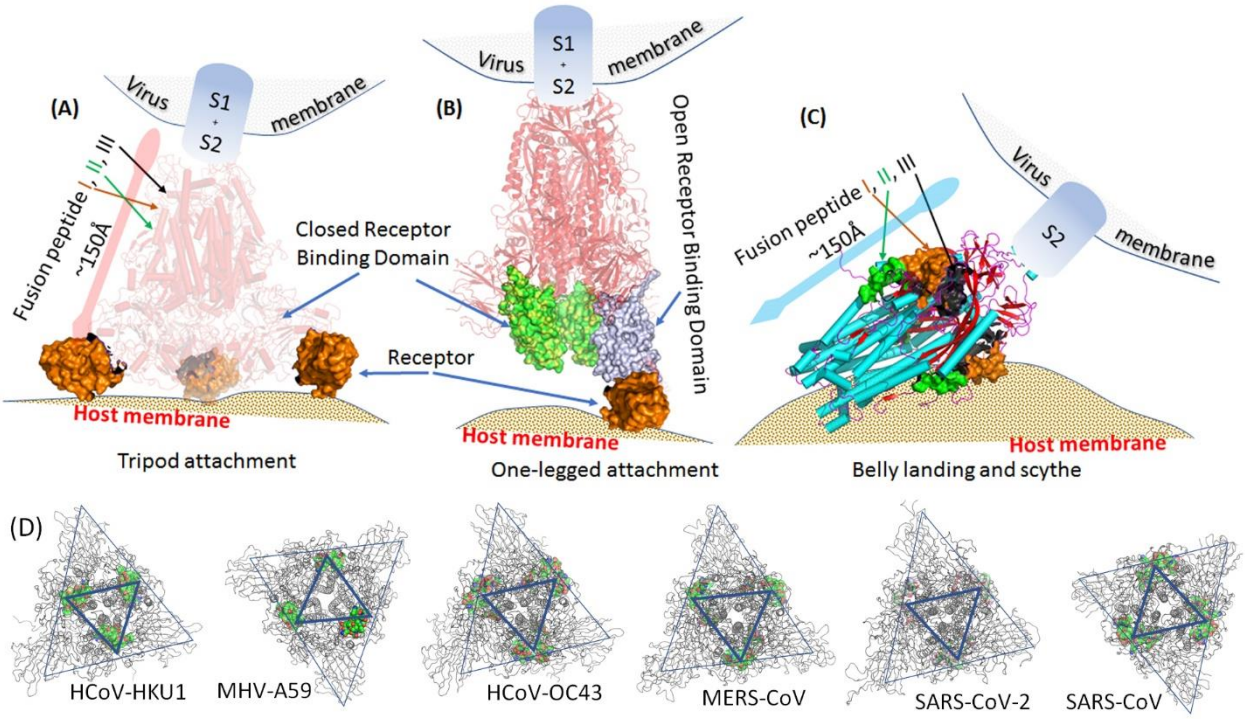
(A)
Virus
S1
+
S2
membrane
I, II, III
Fusion peptide
~150Å
Closed Receptor
Binding Domain
Receptor
Host membrane
Tripod attachment
(B)
Virus
S1
+
S2
membrane
Open Receptor Binding Domain
Host membrane
One-legged attachment
(C)
Virus
S2
membrane
Fusion peptide
I, II, III
~150Å
Host membrane
Belly landing and scythe
(D)
HCoV-HKU1
MHV-A59
HCoV-OC43
MERS-CoV
SARS-CoV-2
SARS-CoV

Fig. 3.

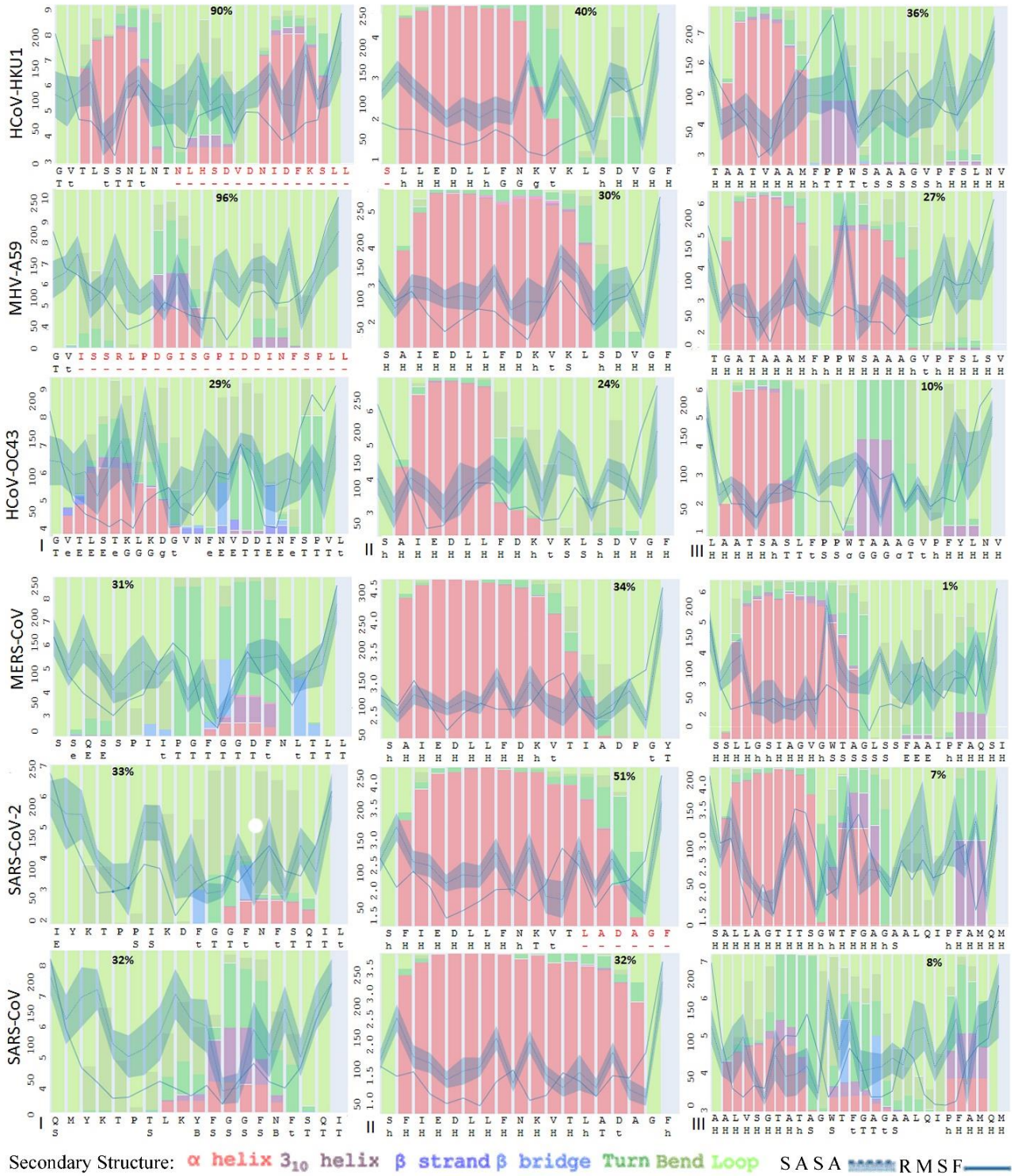
HCoV-HKU1
MHV-A59
HCoV-OC43
MERS-CoV
SARS-CoV-2
SARS-CoV
Secondary Structure: α helix 3₁₀ helix β strand β bridge Turn Bend Loop SASA RMSF

Fig. 4.